Combustion and Flame 158 (2011) 1624–1630

Contents lists available at ScienceDirect

Combustion and Flame

journal homepage: www.elsevier.com/locate/combustflame

Evolution of the nanostructure, fractal dimension and size of in-cylinder soot during diesel combustion process

Zheng Li, Chonglin Song *, Jinou Song, Gang Lv, Surong Dong, Zhuang Zhao

State Key Laboratory of Engines, Tianjin University, Tianjin 300072, China

ARTICLE INFO

Article history:
Received 6 July 2010
Received in revised form 28 November 2010
Accepted 7 December 2010
Available online 4 January 2011

Keywords:
Diesel engine
In-cylinder particle
Nanostructure
Fractal dimension
Primary particle size

ABSTRACT

The nanostructure, fractal dimension and size of in-cylinder soot during diesel combustion process have been investigated for a heavy-duty direct injection diesel engine, using a total cylinder sampling system followed by high-resolution transmission electron microscopy and Raman scattering spectrometry. Different structural organizations of in-cylinder soot are found depending upon the combustion phase. It is revealed that both the fringe tortuosity and separation distance decrease as combustion proceeds, while the mean fringe length increases distinctly from 1.00 to 2.13 nm, indicating the soot evolution toward a more graphitic structure during the combustion process. The fractal dimensions of aggregates are in a range of 1.20–1.74 at various crank angles under the applied engine operating conditions. As temperature and pressure increase, the fractal dimension decreases significantly to a minimum at the early diffusion combustion stage. The soot particles become more compact again as the fractal dimension increases during the subsequent combustion period. Primary particle sizes start small, go through a maximum in the early diffusion combustion phase and decline again as combustion proceeds.

1. Introduction

Diesel soot is known to be agglomerates consisting principally of spherical primary particles with diameters of 15–70 nm [1–3] and possessing characteristic structural properties. At a nanometric scale, a diesel primary particle presents two distinct parts: an inner core and an outer shell, each with different structures [4]. In the characteristic shell/core nanostructure, graphene layers are arranged parallel to the external surfaces in the outer shell, but are randomly arranged with a turbostratic state in central core region [4–7]. Generally, the nanostructure of soot depends strongly on the initial fuel identity and synthesis conditions, such as burning temperature, residence time, fuel properties and fuel/oxygen ratio [8–12], and the nanostructure in turn affects the oxidation reactivity of the soot [13–17]. In addition, the primary particle size and fractal dimension are two important structural parameters for understanding of diesel soot growth processes [18–21].

The structural properties of flame-generated soot [9,11–13] and diesel exhaust soot particles [2–7] have been studied extensively using a variety of fuels and techniques, while investigations of in-cylinder diesel soot have rarely been conducted owing to the high-pressure and high-temperature environment. The diesel in-cylinder soot can differ significantly from laboratory flame-generated soot owing to differences in the fuel composition, the combustion process and the combustion temperature [7], which govern the structural properties of soot (e.g., nanostructure) as mentioned above. The studies of diesel exhaust soot particles may only characterize the structural properties of mature soot emitted from the engines, and thus give little information on the actual soot formation process. Based on this background, we have developed a total cylinder sampling system to obtain diesel in-cylinder soot samples. With this sampling apparatus and microscopic analysis systems, the nanostructure, primary particle size and fractal dimension of in-cylinder soot in different combustion phases have been analyzed for a heavy-duty diesel engine. The degree of graphitization of the in-cylinder soot particles has been determined by Raman spectroscopy. The database obtained from this investigation will provide a better understanding of the formation and oxidation of soot particles inside diesel engine combustion chamber, and optimization of the combustion process to suppress soot formation.

2. Experimental methods

A 5.79 L heavy-duty diesel engine with six cylinders was used for sampling soot from the combustion chamber. The engine was equipped with a common-rail direct fuel injection system and a turbocharged/inter-cooled air intake system, and powered up to 132 kW at a maximum speed of 2600 rpm. The sixth cylinder was extensively modified to develop a total cylinder sampling system (TCSS). The schematic diagram of the TCSS is shown in Fig. 1.

* Corresponding author. Fax: +86 22 27403750.
E-mail address: songchonglin@tju.edu.cn (C. Song).

0010-2180/$ - see front matter © 2010 The Combustion Institute. Published by Elsevier Inc. All rights reserved.
doi:10.1016/j.combustflame.2010.12.006

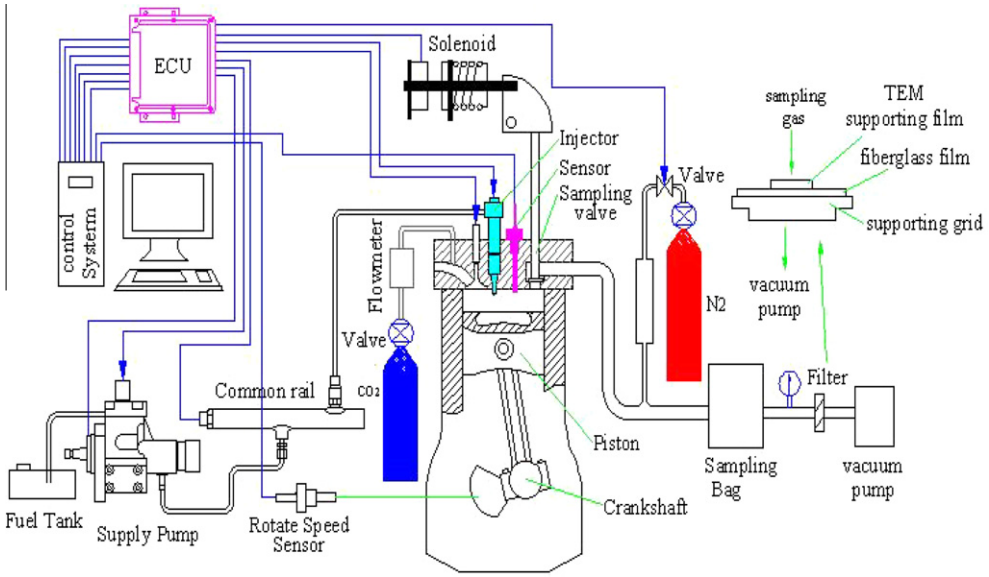

Fig. 1. Schematic diagram of the total cylinder sampling system.

Before each experiment, the sampling bag (the interior of which was coated with aluminum foil to minimize soot loss) and lines were cleaned with high-pressure nitrogen to remove deposited soot particles. The engine was warmed up by running with a low-sulfur diesel fuel for about 30 min to stabilize the operating conditions. Table 1 summarizes the engine operating conditions in current tests. During each total cylinder sampling experiment, the entire cylinder contents were rapidly dumped and collected into the sampling bag at pre-set crank angles at a time scale of 1 ms. Simultaneously, the samples were quenched and diluted by mixing with high-pressure nitrogen at a dilution ratio (DR) of 120:1 to attain a temperature below 52 °C. Diesel soot particles were collected onto the high-resolution transmission electron microscopy (HRTEM) grid and quartz fiber filters (QAT-UP, PallGelman), then stored in protective storage. High dilution of samples at appropriate temperatures could prevent soot condensation and renucleation during the sampling process [22]. To estimate the effect of DR on the aggregate size distributions, the size distributions of exhaust particles at the dilution ratios of 120:1, 300:1, 600:1, 800:1 and 1000:1 were measured by a standard scanning mobility particle sizing system (SMPS, TSI 3090). Engine operating condition was fixed at fuel–air equivalence ratio (ϕ) = 0.41 and engine speed = 1000 rpm. The relative error of mean particle size between DR 120:1 and 1000:1 was less than 5%. In addition, smaller DR could shorten the sampling time, which abated further aggregation. Consequently, DR = 120:1 was employed in this study. The TCSS was further developed on the basis of previous studies [23,24] with a more accurate electric control system. Detailed descriptions of the experimental setup and sampling process were given by Du and Kittelson [23]. Because of the heterogeneous nature of diesel combustion [3,25], a total cylinder sample may contain soot precursors and soot particles at various stages of formation and growth. Therefore, this paper reports the evolution of statistical properties of in-cylinder soot particles (i.e. typical properties of most soot particles) during diesel combustion process. The in-cylinder gas pressure (P), temperature (T), and apparent heat release rate (AHRR) are shown in Fig. 2 for the applied engine conditions. The figure illustrates the different diesel combustion phases (e.g., see Heywood [25] for a detailed definition).

HRTEM and TEM images were acquired using an HRTEM (Philips Tecnai F20) with a point resolution of 0.248 nm operating at 200 kV. Different magnifications were used in the TEM and HRTEM inspections: 20,000× to image the soot morphologies and above 500,000× for measurement of the primary particle (spherule) sizes and nanostructure. The HRTEM images were then digitized and analyzed using an image processing system. For accurate analysis of the soot nanostructure, automated fringe image processing software (FIPS) was developed to obtain quantitative data of the nanostructure parameters, namely the fringe length, separation distance and tortuosity. The FIPS involves separate steps of image normalization, segmentation, enhancement, binary image conversion, skeletonization, post-processing, and quantitative analysis of nanostructure parameters. Fringe length is calculated by automatically counting the number of pixels along a fringe and computing the length using a calibrated pixel size. Fringe tortuosity is obtained by calculating the ratio of the fringe length to the straight-line distance between the endpoints of the fringe. To obtain fringe separation distance, each pair of fringes is manually chosen and then the program gives the mean separation distance of each fringe pair by averaging all separations between the closest points of each pair. More detailed information on these analysis methods has been given in the literature [10–13]. In addition to the HRTEM image analysis, a Raman scattering spectrometer (Renishaw RM1000) was employed to complementarily characterize the soot nanostructure. As classically done with Raman spectral analysis, Raman spectra were recorded over a wavelength number range of 900–2000 cm^{-1} and the magnitude of scanning area was 2-μm in diameter. Experimental uncertainties (95% confidence interval) were estimated to be within 20% for nanostructure

Table 1
Diesel engine operating conditions.

Engine speed (rpm)	Common rail pressure (MPa)	Start of injection (°CA ATDC)	Duration of injection (ms)	Equivalence ratio, ϕ	Intake temperature (K)
1000	90	−8	0.75	0.41	318
1000	90	−8	0.90	0.53	318

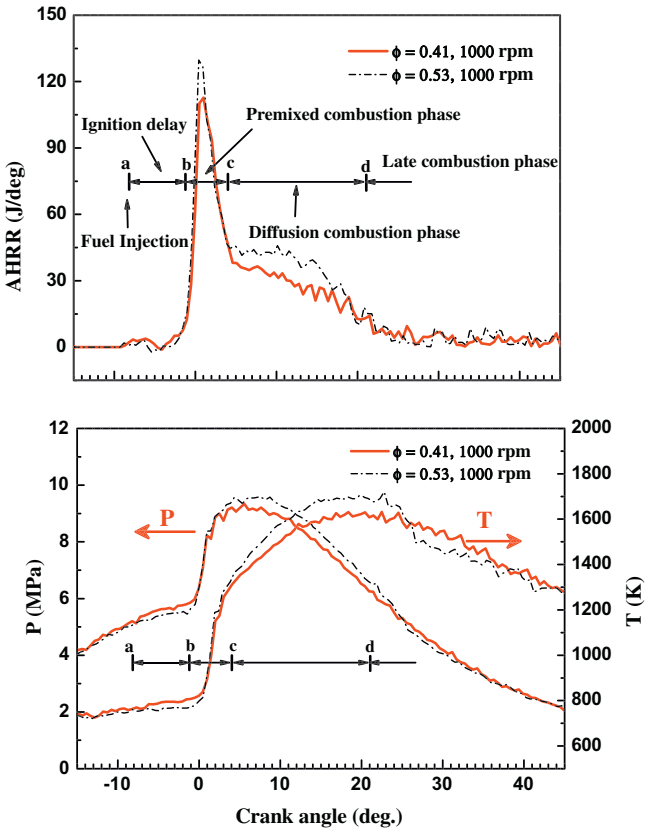

Fig. 2. In-cylinder gas pressure, temperature, and apparent heat release rate diagram identifying different diesel combustion phases.

parameters, 20% for fractal dimension and 15% for primary particle diameter, which were dominated by the finite number of soot particles measured, sampling process, and image analysis biases.

3. Results and discussion

3.1. Nanostructures of in-cylinder soot

HRTEM has become the preferred approach to characterize soot nanostructures because it can readily reveal subtle differences in nanostructure and accurately measure major nanostructural parameters (i.e., the layer fringe length, separation distance and tortuosity) [10–13]. As Raman scattering spectroscopy is known to be sensitive to the structural changes and has been routinely used before [2,14,26], a Raman scattering spectrometer (RSS) is employed in the present study to qualitatively analyze the soot nanostructure based on the relative intensities of the D and G peaks.

Figure 3 presents typical HRTEM images of diesel soot particles in different combustion phases, sampled at $\phi = 0.41$, 1000 rpm. As seen visually, all the soot produced at different combustion timings appear as stacked graphitic lamellas with discernible lengths and stacking orders. Soot particles produced in the premixed combustion phase (Fig. 3a) exhibit lamellas with incoherent orientation and no obvious single center of concentric shell, and display nebulous boundaries. Extended graphene layers and distinct boundaries (Fig. 3b) are observed as combustion proceeds, and evident centers (Fig. 3c, marked by arrows) and characteristic shell/core nanostructure can be noted in late combustion phase soot particles. This shell/core nanostructure might result from the equilibrium configuration of spherical ensembles of nearly planar graphene layers with reactive edges under the high-temperature reactive conditions in the diesel engine [5]. Similar results have been found in previous studies of diesel [10,14] and premixed flame soot particles [11–13], but the observations contradict literature [1] that suggests that no graphitic structure can be distinguished from the HRTEM observation of medium-duty diesel soot particles.

To quantitatively characterize the nanostructural evolution of diesel soot during the combustion process, more than 100 primary soot particles were randomly selected from different aggregates and studied for each crank angle (CA). The fringe length (the extent of the graphene layers), separation distance (the mean distance between adjacent layer planes) and tortuosity (the ratio of the actual fringe length to the straight-line distance) were measured by subsequent image processing using the FIPS. Figure 4 summarizes these structural parameters in different combustion phases as histograms. As shown in Fig. 4a, there is a distinct difference between the fringe lengths (La) in different combustion phases. The soot particles generated at the 0°CA after top dead center (ATDC) have a very narrow distribution with more than 90% of the fringes in a range of 0–1.5 nm in length, while a substantial fraction (>40%) of fringes are longer than 1.5 nm for soot particles produced at 45° ATDC (in the late combustion phase). The graphene layers with planar dimensions consist of carbon atoms located at basal plane and edge-site positions, and the reactivity of basal plane carbon atoms is far lower than that of edge-site carbon atoms [10,11]. Longer fringes correspond to larger graphene layers, and hence to a greater proportion of carbon atoms at basal plane positions. Consequently, more soot particles with ordered structure and lower reactivity exist in the late combustion phase.

Fringe separation distances (d) are presented in Fig. 4b as distribution histograms for the different aging soot particles. As expected from the observation of the HRTEM images shown in Fig. 3, the breadth of the separation distance distribution tends to decrease, and the mean shifts toward smaller values as the combustion proceeds, reflecting soot structures with decreasing interplanar spacing. It has been suggested that larger separation could promote the access of oxygen to the edge-site positions, which could result in higher reactivity [10]. Consequently, soot particles in diesel engine might become less reactive with an increase in CA. In contrast to the results obtained in the present in-cylinder study, a fixed separation distance was found for soot particles of different ages in a premixed flame study [12], which should be attributed to the well-formed structure of young soot particles and relatively low-temperature combustion environment.

Figure 4c plots the histograms of the fringe tortuosity (T_f). A progressive decrease in T_f accompanying the combustion process is evident, with the peak value shifting from 1.4 to 1.1. This reveals that the in-cylinder combustion condition might stabilize the soot to an ordered structure because higher tortuosity indicates that there are more odd-membered rings within the carbon planes and that there is an increase in the sp^2/sp^3 hybridization ratio, reflecting less electron resonance stabilization [10–13].

The mean values of these nanostructure parameters versus CA are shown in Fig. 5. In general, both the T_f and d decrease as combustion proceeds, while the La increases distinctly from 1.0 to 2.13 nm. With an increase in CA, soot particles will therefore possess more carbon lamellas with small numbers of active edge-site carbon atoms [17], smaller separations and fewer odd-membered carbon rings with weak C–C bonds [10]. These results demonstrate the soot evolution toward better graphitic organization and higher resistance to oxidation during the combustion process. It is speculated that these trends are due to three basic processes:

(1) The high-temperature flame environment facilitates the pyrolysis of fuel into smaller species, which can build and coalesce to form highly ordered graphene layers [11,12].

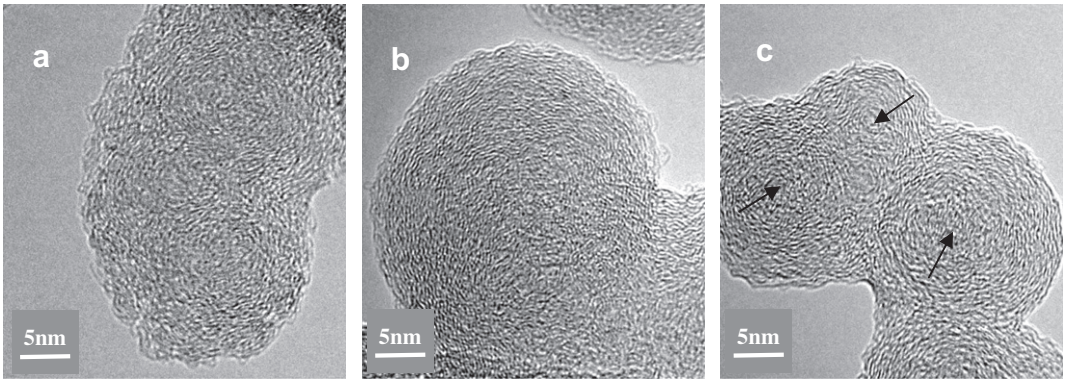

Fig. 3. Typical HRTEM images of in-cylinder diesel soot sampled at: (a) 0°CA ATDC, (b) 11°CA ATDC and (c) 45°CA ATDC for $\phi = 0.41$.

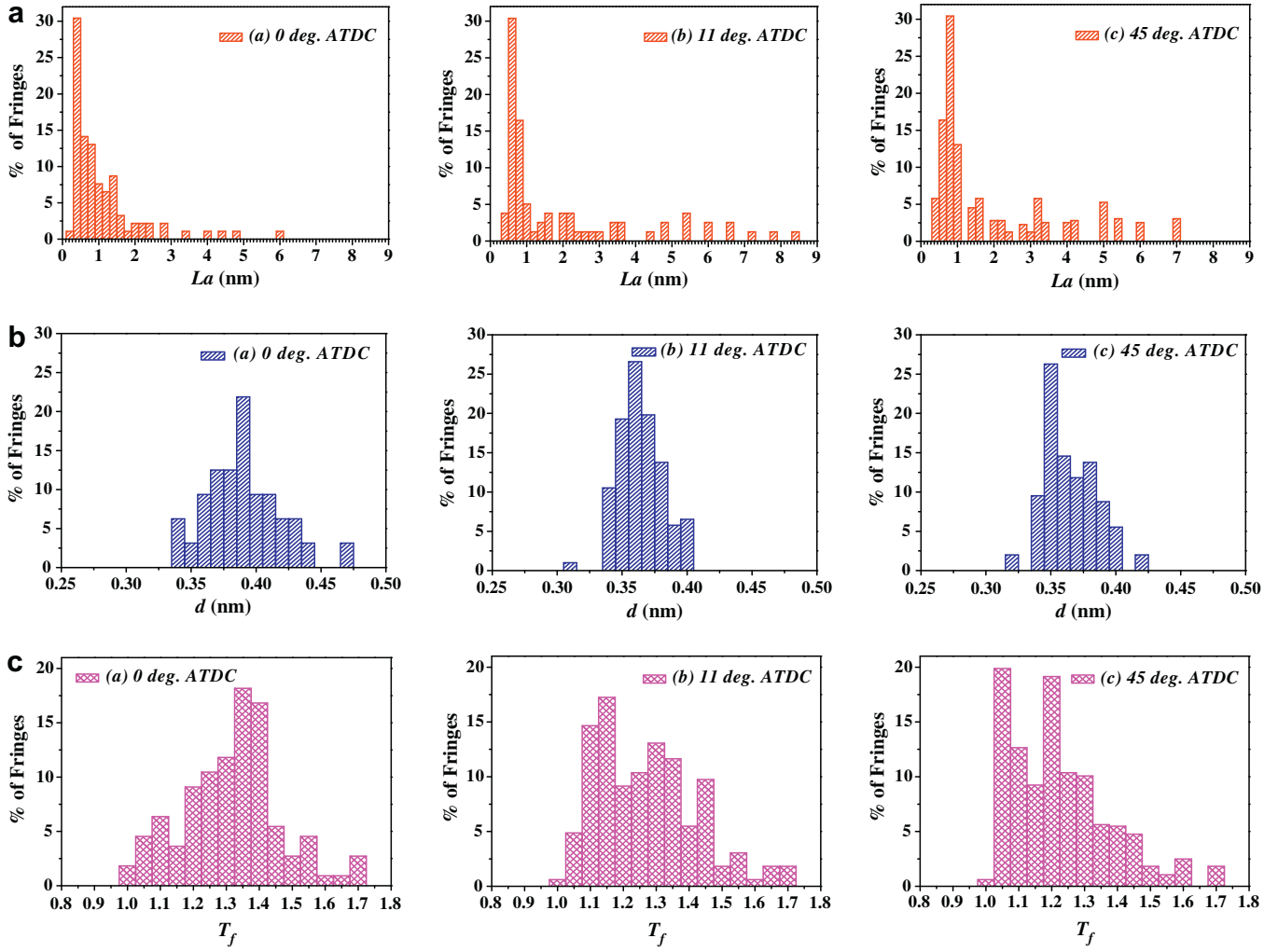

Fig. 4. Histograms of the graphitic layer plane fringe length (La), separate distance (d) and tortuosity (T_f) analyzed from the corresponding images.

(2) The long residence time of the early formed soot at higher temperature promotes further oxidation of the short and disordered carbon layers near the soot boundaries [14].
(3) As temperature increases, crystallite grows in-plane via the incorporation of existing graphene layers and non-organized carbon and coalescence of crystallites with a side-by-side junction of the graphene layers [27].

Besides the overall trends of the structural parameters, it is also interesting to note that there are distinctly different evolution stages of soot nanostructure through the combustion process. In the early premixed combustion phase, the soot particles consist of short and randomly oriented graphitic segments, and there is a rapid change in the structural parameters as combustion proceeds. The significant change in the premixed combustion phase

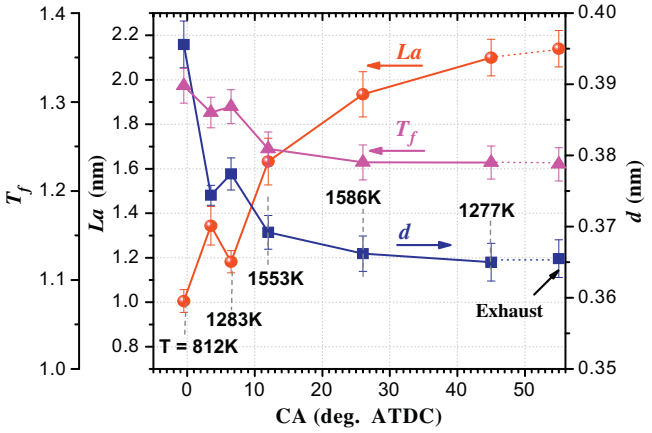

Fig. 5. Mean fringe length (La), separate distance (d) and tortuosity (T_f) as functions of CA. The error bars indicate the standard error in the measurements.

is mainly attributed to the high activity of these early forming soot particles, where the outermost amorphous shell is easily removed by enhanced oxidation at rapidly increasing temperature [14]. As the AHRR is controlled primarily by diffusion combustion [25], a slight decrease in La and a slight increase in d are observed at 4–7°CA ATDC, indicating a decrease in the structural order to some extent. In this case, the great number of newly generated soot particles with amorphous structure is the predominant factor. In the CA range of 7–22° ATDC, it is speculated that high temperature and long residence time are responsible for the gradual decrease in the structural disorder. Since soot particles have become stable and less active, a further change in particle nanostructure becomes extremely difficult [11]. In the late combustion phase, soot particles exhibit a well-formed graphitic structure and do not distinctly change since the dramatic decrease in in-cylinder pressure and temperature cannot provide sufficient thermal activation energies for further change of the soot structure [11,27].

The Raman spectra of soot particles for different crank angles are plotted in Fig. 6 to supplement the nanostructure information and validate the previous results of HRTEM. All spectra present two distinct peaks: G (graphitic) peaks at 1591.5 cm^{-1} and D (defect) peaks at 1348.4 cm^{-1}. While the G peaks have an almost constant intensity of about 4137.27 arb.unit, the intensities of D peaks clearly decrease from 3836.97 to 3393.28 arb.unit with an increase in CA. In the Raman spectra, the G peak is related to a C–C stretching motion along the longitudinal axis of the graphitic plane, and the D peak originates from the breakdown of the selection rules for graphene atoms in the breathing vibrational mode, with an intensity that depends on the disorder level of the graphitic structure [14,28]. The relative D peak to G peak intensity (I_D/I_G) is directly related to the size and defects in the basal plane of the graphene layers (i.e., follow equation: $I_D/I_G = C/La$, where C is a constant [2]). Therefore, the striking feature of the gradual decrease in the intensity of the defect peak indicates the tendency of soot structure toward a more ordered state and/or the oxidation of the amorphous portions of the soot particles during the combustion process. The values of I_D/I_G were also calculated and a fairly linear relation with $1/La$ was attained, which testifies the characterization of nanostructure above-mentioned.

3.2. Aggregate fractal dimensions

Though diesel soot particles have a broad size distribution and widely varying shape, the complex geometry of typical aggregates are normally characterized as mass fractal. The fractal dimension (D_f) has been widely used to describe the geometric and aerodynamical properties of soot in many combustion environments [1,2,22]; however, few studies have measured the fractal properties during the diesel combustion process. In the present in-cylinder study, the fractal dimensions were calculated and recovered from two-dimensional TEM images with formulas widely used in past studies. Detailed descriptions of the measurement procedures can be found in the literature [1,2,26].

To investigate the soot fractal feature during the combustion process, about 600 aggregates were randomly acquired to attain reasonable statistical data for each sampling condition. The number of spherules in each aggregate selected is found to fall in the range from 40 to 200. Fig. 7 presents the D_f as a function of CA for two different engine operating conditions. In the premixed combustion phase (at 1°CA ATDC), with low temperature and pressure (T = 830 K, P = 6.4 MPa), the fractal dimensions are relatively high (D_f = 1.74, 1.63) indicating a compact soot morphology. As the combustion proceeds from the premixed phase to the early diffusion phase, the temperature, pressure and the number of soot particles formed newly increase rapidly, and the D_f decreases significantly to a minimum due to poor agglomeration for these new soot particles at this very short period [2,29]. The low D_f implies more soot particles with chain-like structure (see Fig. 8a). During the subsequent combustion period, corresponding to much lower AHRR and few newly formed soot particles, an increase in D_f is observed with a decrease in cylinder pressure, signifying that the in-cylinder soot particles are more compactly clustered (see Fig. 8b).

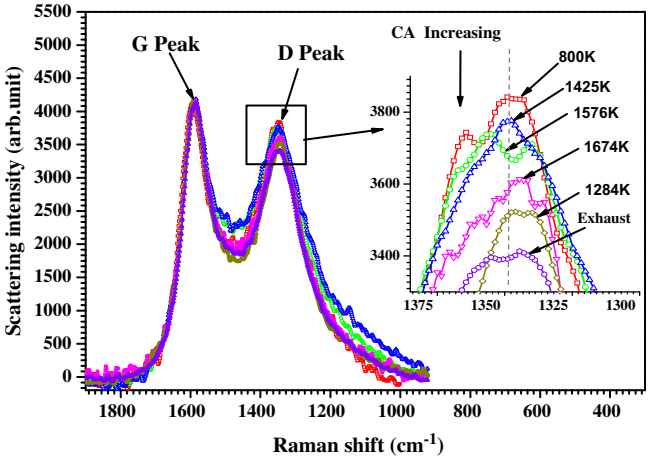

Fig. 6. Raman spectra of soot particles for different CAs at ϕ = 0.41, 1000 rpm.

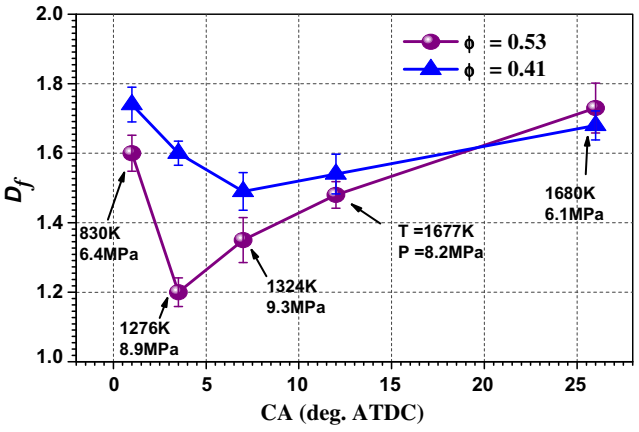

Fig. 7. Fractal dimension (D_f) of soot particles as a function of CA at 1000 rpm. The error bars represent the standard error.

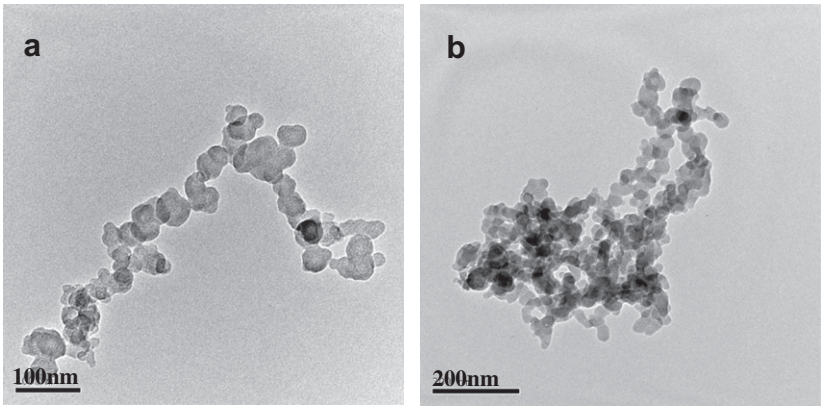

Fig. 8. Typical TEM images of in-cylinder diesel soot sampled at (a) 3.5°CA ATDC, (b) 26°CA ATDC for $\phi = 0.53$.

The minimum soot fractal dimension at $\phi = 0.53$ is much lower than the value at $\phi = 0.41$. The discrepancies may relate to the differences in the newly generated soot particles at this stage. On the one hand, when AHRR is controlled primarily by diffusion combustion [25], more soot particles for $\phi = 0.53$ are generated than those for $\phi = 0.41$ at this stage because high equivalence ratio promotes the increment of particles in number. On the other hand, the fractal dimension values of these new soot particles are relatively small due to poor agglomeration at this very short period [2,29]. Accordingly, the value of fractal dimension for $\phi = 0.53$ is smaller than that for $\phi = 0.41$ at this period. The dependence of D_f upon engine loads was also reported in previous exhaust studies and attributed to different levels of volatile mass [2] or sulfate [30,31]. Although the fractal dimension widely varies from 1.2 to 1.74 during the combustion process, it shifts toward an approximate value of 1.70 in the late combustion phase, in excellent agreement with the fractal dimension value reported in recent studies of exhaust particles [1,2]. However, in several studies [30,31] the fractal dimension (D_{fm}) was measured by mobility instruments, which substantially varied from 2.1 to 2.9. In fact, D_{fm} should not be confused as the fractal dimension (D_f) measured by TEM. Mobility measurements adopt the soot particles condensed with much volatile liquid and the hypothesis of spherical geometry [26] while volatile materials on the soot particles will vaporize promptly during TEM measurement procedure.

3.3. Primary particle size measurement

Similar to past TEM observations of laboratory flames [9,26] and exhaust gas [1,2], in-cylinder diesel soot particles were inspected as aggregates in fractal-like morphology composed of almost spherical primary particles (spherules). Diameters of primary particles were visually determined by selecting the same area of primary particles as the projected area with the image processing system [1,2]. For the measurement of primary particle size, more than 150 spherules were randomly selected from different aggregates for each CA and engine condition, and primary particles with unclear boundaries were omitted to minimize experimental error. In Fig. 9, the mean primary particle diameters (d_p) are plotted as a function of CA for two different fuel–air equivalence ratios at 1000 rpm. The average spherule diameters range from 18 to 29 nm during combustion process under all engine operating conditions. Primary particles are initially small (21–22 nm), then enlarge to a maximum size during the early diffusion combustion phase, and subsequently become smaller as the combustion proceeds.

In light of what is known of soot formation [1,2,22,28], the primary particle size mainly depends on the competition between soot oxidation and surface growth, which is greatly affected by the combustion conditions. In the early combustion phase, the mean primary particle size increases significantly as temperature and pressure increase rapidly, which can be attributed to the dominant surface growth for most primary particles [1,2]. As combustion proceeds, the mean primary particle sizes for both fuel–air equivalence ratios reach their maxima (26 and 29 nm, respectively) in the early diffusion combustion phase and then decrease, mainly owing to the high soot oxidation rate under the high-temperature condition and the decrease in net soot formation [2,3,24]. Indeed, it has been speculated in laboratory flame studies that the rate of soot oxidation increases more rapidly than the rate of formation as temperature increases, and the net soot formation decreases after reaching a maximum [3].

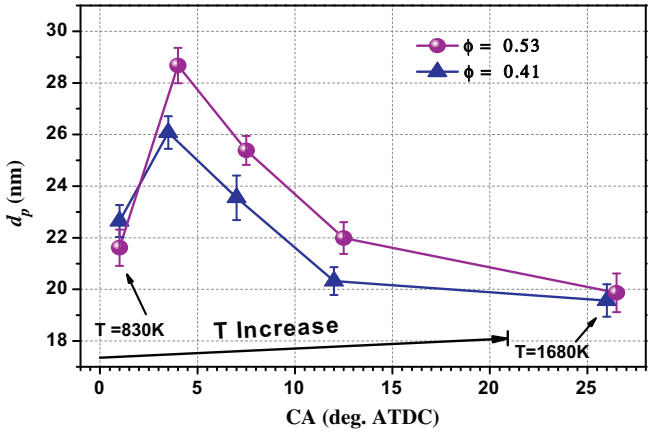

Fig. 9. Mean primary particle diameter (d_p) as a function of CA at 1000 rpm. The error bars indicate the standard error in the measurements.

The influence of ϕ on the average spherule diameter during the combustion process can also be observed in Fig. 9. It is clear that the primary particle diameter for $\phi = 0.53$ is greater than that for $\phi = 0.41$ in most cases, which is in agreement with the findings of Neer et al. and Zhu et al. [1,2]. A higher fuel–air ratio not only suppresses soot oxidation but also enhances soot nucleation and surface growth [1,2]. Additionally, it can be seen in Fig. 8 that the mean diameters of primary particles for both $\phi = 0.53$ and $\phi = 0.41$ are approximately equal at the late combustion phase (at 27°CA ATDC).

4. Conclusions

The soot fractal dimension, primary particle size and nanostructure during the diesel combustion process have been

systematically characterized by total cylinder sampling followed by HRTEM and RSS analysis. Different structural organizations of diesel soot particles are found in the different combustion phases. Both the fringe tortuosity and separation distance decrease as combustion proceeds, while the fringe length increases distinctly from 1.00 to 2.13 nm, which indicates that soot particles shift toward better graphitic organization and higher resistance to oxidation. Furthermore, the soot nanostructure presents different evolution stages through the combustion process. Under the applied engine operating conditions, the fractal dimension of in-cylinder soot particles is in the range of 1.2–1.74 during the combustion process. The fractal dimension significantly decreases to a minimum value as the temperature and pressure increase, implying the production of aggregates that are more loosely packed and chain-like, and then increases with a decrease in pressure, signifying the in-cylinder soot particles are more compactly clustered in the late combustion phase. The mean diameters of primary particles for both $\phi = 0.41$ and $\phi = 0.53$ range from 18 to 29 nm during the combustion process. The mean sizes of primary particles start small and increase to a maximum during the early diffusion combustion phase. Subsequently, the primary particle sizes decrease as the combustion proceeds due to the high soot oxidation rate and the weakening of net soot formation.

In general, a multistage history is found for the evolution of the in-cylinder soot properties through the diesel combustion process. In this study, both the fractal dimension and primary particle diameter reach extrema in the early diffusion combustion phase (at about 4–7°CA ATDC), and the evolution of in-cylinder soot nanostructure presents different stages during the combustion process.

Acknowledgments

This study was supported by the National Natural Science Foundation of China (No. 51076116) and the State Key Laboratory of Engines at Tianjin University.

References

[1] A. Neer, U.O. Koylu, Combust. Flame 146 (1–2) (2006) 142–154.
[2] J. Zhu, K.O. Lee, A. Yozgatligil, M.Y. Choi, Proc. Combust. Inst. 30 (2) (2005) 2781–2789.
[3] D.R. Tree, K.I. Svensson, Prog. Energy Combust. Sci. 33 (3) (2007) 272–309.
[4] T. Ishiguro, Y. Takatori, K. Akihama, Combust. Flame 108 (1–2) (1997) 231–234.
[5] R.H. Hurt, G.P. Crawford, Hong-Shig Shim, Proc. Combust. Inst. 28 (2) (2000) 2539–2546.
[6] H.X. Chen, R.A. Dobbins, Combust. Sci. Technol. 159 (1) (2000) 109–128.
[7] A.D.H. Clague, J.B. Donnet, T.K. Wang, J.C.M. Peng, Carbon 37 (10) (1999) 1553–1565.
[8] U. Mathis, M. Mohr, R. Kaegi, Environ. Sci. Technol. 39 (2005) 1887–1892.
[9] R.A. Dobbins, C.M. Megaridis, Langmuir 3 (1987) 254–259.
[10] R.L. Vander Wal, C.J. Mueller, Energy Fuel 20 (6) (2006) 2364–2369.
[11] R.L. Vander Wal, A.J. Tomasek, Combust. Flame 136 (1–2) (2004) 129–140.
[12] M. Alfè, B. Apicella, R. Barbella, J.N. Rouzaud, A. Tregrossi, A. Ciajolo, Proc. Combust. Inst. 32 (1) (2009) 697–704.
[13] R.L. Vander Wal, SAE Technical Paper 2005–01–0964.
[14] J. Song, M. Alam, A.L. Boehman, U. Kim, Combust. Flame 146 (4) (2006) 589–604.
[15] T. Ishiguro, N. Suzuki, Y. Fujitani, H. Morimoto, Combust. Flame 85 (1–2) (1991) 1–6.
[16] D.S. Su, J.O. Müller, R.E. Jentoft, D. Rothe, E. Jacob, R. Schlögl, Top. Catal. 30/31 (1) (2004) 241–245.
[17] R.L. Vander Wal, A.J. Tomasek, Combust. Flame 134 (1–2) (2003) 1–9.
[18] B. Bougie, L.C. Ganippa, A.P. Vliet, W.L. Meerts, N.J. Dam, J.J. Meulen, Proc. Combust. Inst. 31 (1) (2007) 685–691.
[19] K.O. Lee, J.Y. Zhu, S. Ciatti, A. Yozgatligil, M.Y. Choi, SAE Technical Paper 2003–01–3169.
[20] A. Braun, F.E. Huggins, S. Seifert, J. Ilavsky, N. Shah, K.E. Kelly, A. Sarofim, G.P. Huffman, Combust. Flame 137 (1–2) (2004) 63–72.
[21] K.O. Lee, R. Cole, R. Sekar, M.Y. Choi, J.S. Kang, C.S. Bae, H.D. Shin, Proc. Combust. Inst. 29 (1) (2002) 647–653.
[22] H. Burtscher, J. Aerosol Sci. 36 (7) (2005) 896–932.
[23] C.J. Du, D.B. Kittelson, SAE Technical Paper, 1983 (830243).
[24] L. Luo, M.J. Pipho, SAE Technical Paper, 1989 (890580).
[25] J.B. Heywood, Internal Combustion Engine Fundamentals, McGraw Hill, 1988.
[26] M.F. Chandler, Y.W. Teng, U.O. Koylu, Proc. Combust. Inst. 31 (2) (2007) 2971–2979.
[27] F.G. Emmerich, Carbon 33 (12) (1995) 1709–1715.
[28] M.M. Maricq, J. Aerosol Sci. 38 (11) (2007) 1079–1118.
[29] H.W. Kim, M. Choi, J. Aerosol Sci. 34 (12) (2003) 1633–1645.
[30] M.M. Maricq, N. Xu, J. Aerosol Sci. 35 (10) (2004) 1251–1274.
[31] J.S. Olfert, J.P.R. Symonds, N. Collings, J. Aerosol Sci. 38 (1) (2007) 69–82.